Form Approved
OMB No. 0704-0188

1. AGENCY USE ONLY (Leave blank)	2. REPORT DATE	3. REPORT TYPE AND DATES COVERED
	October 29,1992	Reprint

(2)

4. TITLE AND SUBTITLE

Contamination Signatures Observed During the CIRRIS-1A Mission

5. FUNDING NUMBERS

PE 62101F
PR 3054
TA 01
WU 23

6. AUTHOR(S)

Byron David Green*, W. Terry Rawlins*, O. Manuel Uy#, Richard M. Nadile, Ned Wheeler

7. PERFORMING ORGANIZATION NAME(S) AND ADDRESS(ES)

Phillips Lab/GPOB
Hanscom AFB
Massachusetts 01731-5000

8. PERFORMING ORGANIZATION REPORT NUMBER

PL-TR-92-2259

9. SPONSORING/MONITORING AGENCY NAME(S) AND ADDRESS(ES)

10. SPONSORING/MONITORING AGENCY REPORT NUMBER

11. SUPPLEMENTARY NOTES *Physical Sciences, Inc. Andover, MA 01810 #Applied Physics Laboratory, Laurel, MD 20723 - Reprint-Presented at the Cryogenic Optical Systems and Instrumentations V, Technical Conference 1765-SPIE International Symposium on Optical Applied Science and Engineering, San Diego, CA 23-24 July 92

12a. DISTRIBUTION/AVAILABILITY STATEMENT

Approved for public release; Distribution unlimited

12b. DISTRIBUTION CODE

13. ABSTRACT (Maximum 200 words)

The sensitive, high resolution CIRRIS-1A radiometers/interferometer provided a unique capability to probe the optical environment surrounding the shuttle on the STS 39 mission. Ground processing was carefully controlled to minimize the contamination levels. Early in the mission all surfaces were subjected to extended solar exposure. These efforts were successful in that most of the data showed no evidence of contamination effects. However, particulate contamination effects were occasionally observed. The range and size of discrete particles are extracted from the particle radiances, spectral distributions, and blur circles.

14. SUBJECT TERMS

Particulate contamination, Infrared optical near-field environment, CIRRIS-1A, Shuttle environment, Spectra particulate

15. NUMBER OF PAGES

10

16. PRICE CODE

17. SECURITY CLASSIFICATION OF REPORT	18. SECURITY CLASSIFICATION OF THIS PAGE	19. SECURITY CLASSIFICATION OF ABSTRACT	20. LIMITATION OF ABSTRACT
Unclassified	Unclassified	Unclassified	SAR

Contamination signatures observed during the CIRRIS-1A mission

Byron David Green and W. Terry Rawlins

Physical Sciences Inc.
Andover, MA 01810

O. Manuel Uy
Applied Physics Laboratory
Laurel, MD 20723

Richard M. Nadile and Ned Wheeler
Geophysics Directorate/Phillips Laboratory
Hanscom AFB, Bedford 01730

ABSTRACT

The sensitive, high resolution CIRRIS-1A radiometers/interferometer provided a unique capability to probe the optical environment surrounding the shuttle on the STS 39 mission. Ground processing was carefully controlled to minimize the contamination levels. Early in the mission all surfaces were subjected to extended solar exposure. These efforts were successful in that most of the data showed no evidence of contamination effects. However, particulate contamination effects were occasionally observed. The range and size of discrete particles are extracted from the particle radiances, spectral distributions, and blur circles.

1. INTRODUCTION

Spacecraft produced contamination in the optical viewing path surrounding the sensor will obscure or degrade the far field observations. Radiometers will exhibit enhanced background intensities and temporal variability. Imagers will exhibit structured backgrounds and bright streaks by particle tracks. These optical effects will be wavelength dependent.

Particles have been observed on most space missions including the Mercury-Apollo, Skylab, Shuttle (STS-2, -3,-4,-9,-SPACELAB 3,-61C, and -39),[1] and Magellan spacecraft. The shuttle-based film imaging systems have provided the most extensive and best characterized data set.[2-4] For these observations, solar illumination drives the detection limits. Particles larger than 40 μm were detectable at distances of less than 100m. The environment was variable and between 0.3 and 50 particles would be detected per orbit by a 10^{-5} sr detection system. The size distribution peaks to lower radii (indeed a size scaling of $r^{-3/2}$ was extracted from Skylab occultation data).[5] The stereoscopic cameras on the Induced Environment Contamination Monitor pallet[2,3] were able to quantify the observed velocities as in the 0.3 to 3 m/s range. Modeling[6] suggests this reflects a small initial ejection velocity with subsequent drag induced relative acceleration. The PACS data[4] provided insight into the sources of particulates. Activities such as maneuvers, mechanical operations, dumps, and thermal stresses upon terminator crossings induced the release of particles from surfaces. Temperature controlled Quartz Crystal Microbalances on Spacelab 1 provided particle capture directionality and composition.[7] Alumina, Mg, Al, Si, and Cl were observed and attributed to ascent and solid rocket firings. We have previously developed an empirical model of the particulate environment surrounding shuttle.[1]

Particulate contamination can be carried up from the ground or be created by mechanical stresses/wear, erosion, or impacts while on-orbit. Thus, careful ground handling and contamination control procedures may not necessarily ensure a good orbital optical environment.

The CIRRIS-1A instrument provides sensitive monitoring of the infrared optical near-field environment. It provides spectral coverage over the 2.5 to 25 μm region. This broad wavelength coverage on observations of particles permits particle composition to be extracted through analysis.

The primary CIRRIS-1A sensors are a high-resolution Michelson interferometer and a dual channel radiometer sharing common collection optics and telescope. The optics, detectors and preamplifiers are cooled to 12 K to permit faint remote signal detection. An array of five Si:As detectors are at the focal plane of the interferometer. The largest detector has a 10 mr square field of view through the Ritchey-Cretien optics and achieves an NESR of 2×10^{-13} W/cm^2-sr-cm^{-1} at 625 cm^{-1}. The two-channel radiometer contains nine Si:As detectors behind an eight position filter wheel, and five Bi:As detectors sensing 2.7 μm emission. The radiometers achieve NESRs in the 10^{-9} to 3×10^{-12} W/cm^2 sr-μm range. The individual detectors in the radiometer mostly have a vertically oriented 3.0 x 0.5 mr field of view, with the array spanning 20 mr total. Both radiometer focal planes are co-aligned with the interferometer focal plane permitting simultaneous bandpass/spectral measurements. The sensors and cryostat are mounted on a two-axis gimbal system to provide accurate pointing capability. The CIRRIS-1A payload has been described by Ahmadjian et al.[8]

The CIRRIS-1A payload was assembled under carefully controlled conditions at Utah State University. After integration into the bay of Discovery, the entire cargo section was carefully cleaned in the Orbiter Processing Facility and on the pad just prior to launch.

2. ORBITAL DATA ACQUISITION

Shuttle mission STS-39 was launched at 7:35 AM on 28 April 1991. A nominal 260 km orbit was achieved. The payload bay doors were opened at 1:15 after launch. Starting at 3:40 after launch, the orbiter was oriented so that the sun fully illuminated first the orbiter's bottom tiles (+Z) and then the bay (-Z) for a solar illuminated portion of an orbit each. This was an attempt to warm the surfaces and speed removal of the adsorbed water and carbon dioxide. Previous mass spectrometer data from shuttle supports this approach.[9]

The cover to the CIRRIS-1A instrument was opened 20 hours after launch, and acquisition of atmospheric radiance data began almost immediately. The CIRRIS-1A on-orbit operations include vertical, horizontal, and stare scans of the earthlimb and deep space using various filter bandpasses. Observations were performed in the relatively stable gravity gradient mode (nose to earth) looking into the wake with the thrusters disabled. This orientation should minimize any effects of the ram plow cloud (such as glow, atomic oxygen erosion, or cryofilm formation) and of the thrusters (such as cryofilm formation by the backscattered exhaust, or optical interference signatures).

We searched for particulate contamination radiances during periods when the line-of-sight tangent heights were above 200 km and remote atmospheric radiances were small, approaching the background noise levels of the detection system sensitivities. A large particle radiance was observed during an auroral tracking gimbal maneuver at 27:47 (1 day, 3+ hours) after launch. This is during a period of orbital night. Figure 1 displays the radiometer signal levels in the 8.4 to 18 μm bandpass during a 12s period. The observed signal is temporally varying. Although the particle remains in the field of view for about 10s, the detected intensity varies by 30% as the particle rotates. Note that integrated radiances are in the 3 to 7×10^{-4} W/cm^2-sr range for six different detectors. Figure 2 displays the radiances observed on six of the detector elements immediately after the period displayed in Figure 1. For this second

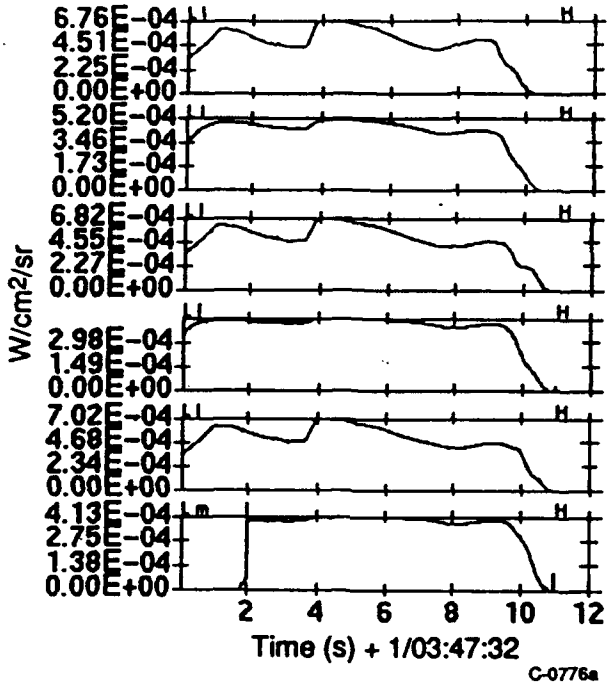

Fig. 1. Intensity signals from LWIR filtered radiometer detectors 1-1 through 1-6 at mission time 1/03:47:32 through :44.

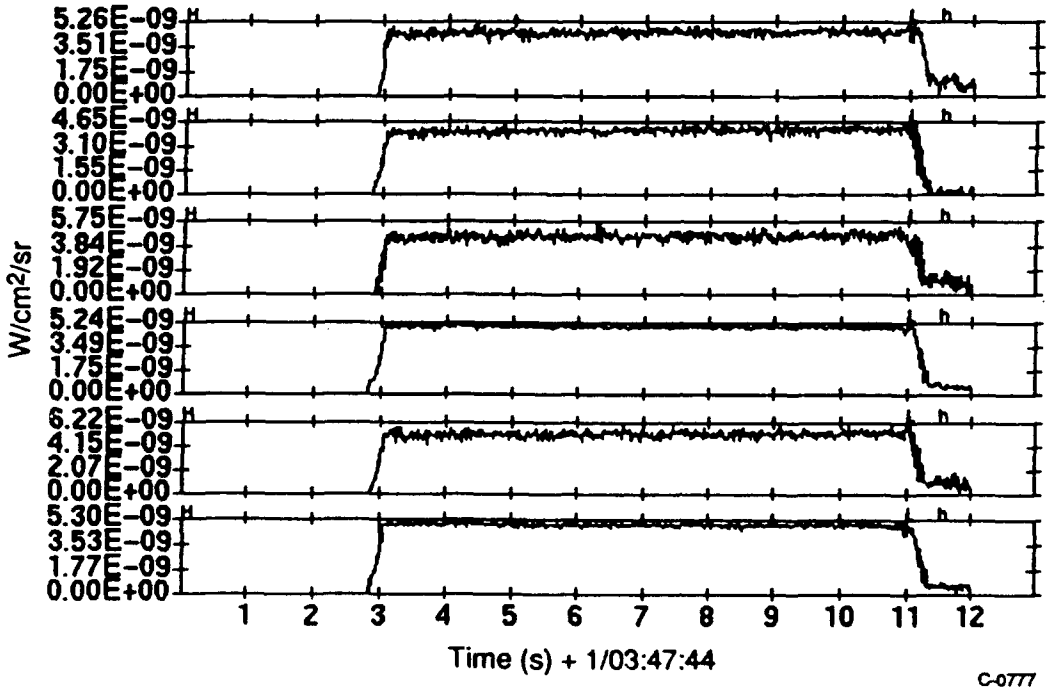

Fig. 2. Intensity signals from LWIR filtered radiometer detectors 1-1 through 1-6 at mission time 1/03:47:44 through :56.

particle, the radiances observed by all detectors are in the 5 x 10^{-9} W/cm^2-sr range. This particle remains in the field of view producing a constant intensity for about 8s.

During this period, the interferometer data displays a bright, spectrally structured emission as shown in Figure 3. The spectra have a spectral resolution of 4 cm^{-1} and take 2.7s to acquire. The displayed intensity corresponds to the instantaneous particle brightness at the center of the interferometer scan, and not an average over the 3s. The spectra acquired during the period of time of the radiometer traces of Figure 1 differ somewhat in spectral shape as shown in Figure 4. The third spectrum was 2.5 times weaker than the first two and exhibits a distinct spectral peak between 7 and 10 μm. The fourth spectrum taken as the particle moved out of the interferometer field of view was not recoverable due to the large intensity changes during the scan. Displayed in Figure 5 is a spectrum acquired during the period corresponding to the radiometer traces shown in Figure 2. Also indicated in Figure 5 is the approximate intensity level of the instrument noise background. Even this small particle produces a spectrum six times the noise level. Our analysis of this data is presented in the next section.

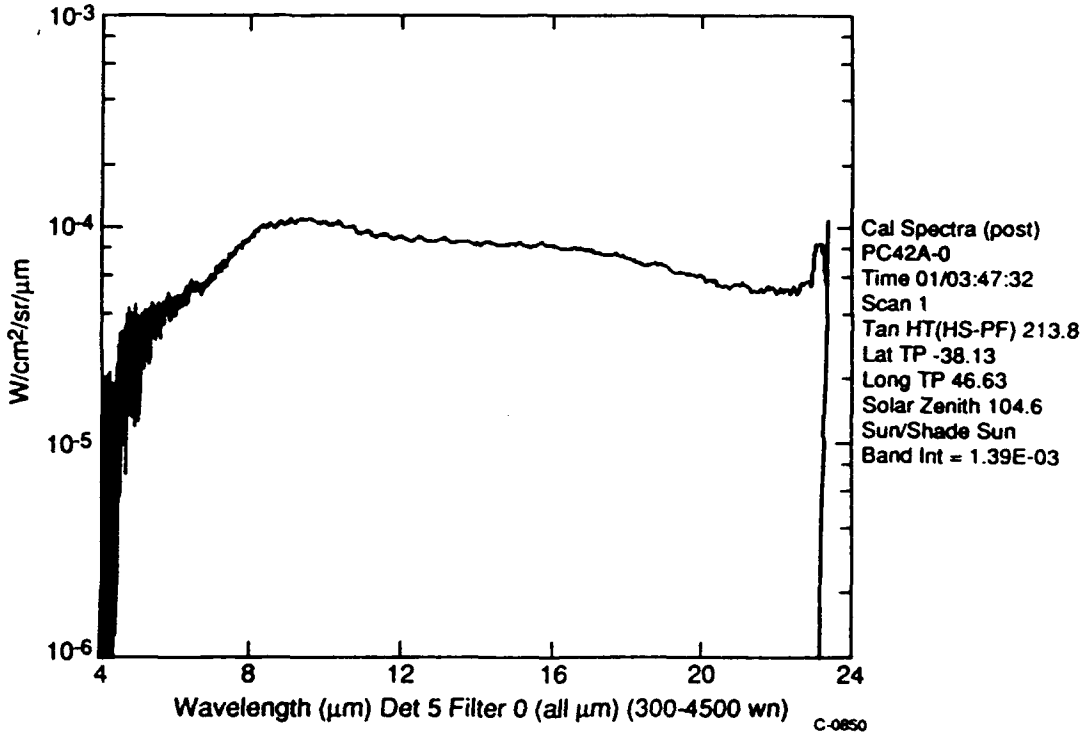

Fig. 3. Spectrum from unfiltered interferometer detector 5 at mission time 1/03:47:32.

3. DATA ANALYSIS

Particles located in the near-field will be out of focus with this telescoped system and the image of the particle at the detection plane will overfill the detectors. As an example, for the 30.48 cm diameter (<700 cm^2) telescoped/baffled detection system for the interferometer, a single detector has an angular resolution of 1.5 and 26 mr.[8] The radiometer consists of 0.5 x 3.0 mr elements, with the array subtending 18 mr. The blur circle from a particle will be comparable in size to the smallest interferometer detector at a distance of 61m, and to the radiometer detectors at a distance of 45m. At all distances inside of this range, the particle's image will spread over several detectors in the array. As the distance of the particle from the sensor decreases, the blur circle will spread over an increasing number of elements. The total intensity of the particle radiance reaching the array increases as the square

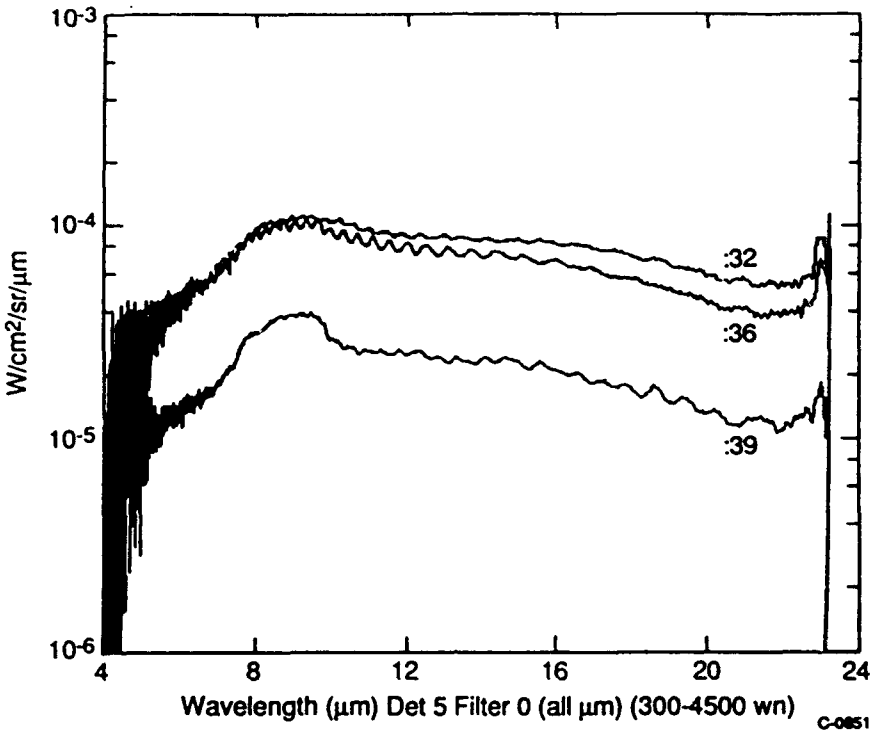

Fig. 4. Spectrum from unfiltered interferometer detector 5 from three sequential scans.

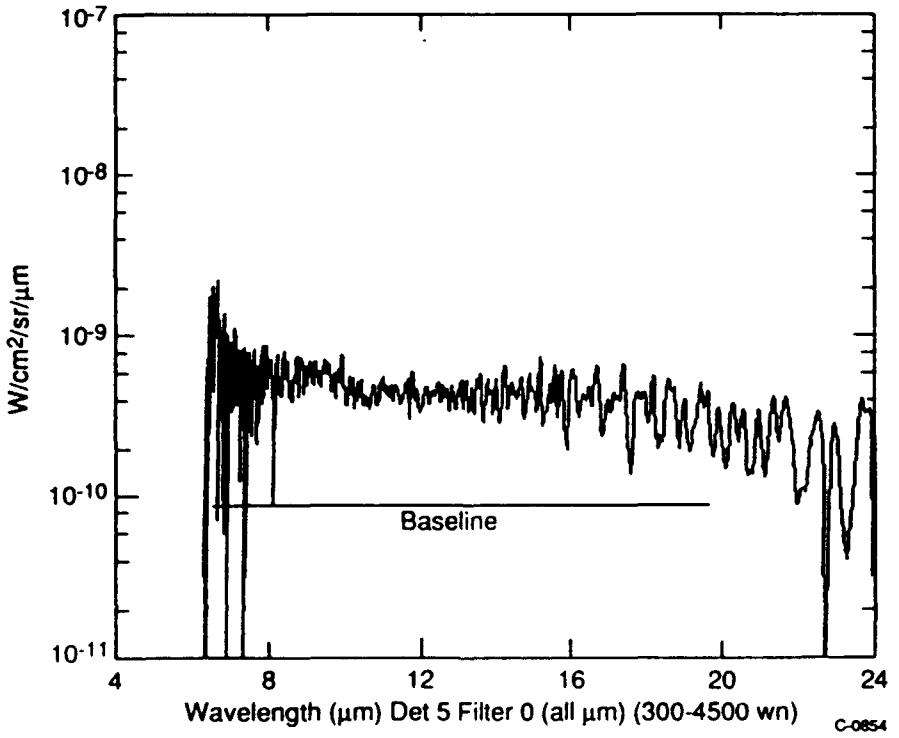

Fig. 5. Spectrum from unfiltered interferometer detector 2 at mission time 1/03:47:54.

of decreased distance. The intensity on a given pixel, however, remains constant with the blur circle size increase offsetting the $1/r^2$ proximity intensity increase. At distances of less than 7.5m, the particle blur circle overfills the arrays. At distances inside the primary collection mirror focal length, the collection efficiency drops off further. Thus telescoped systems are sensitive detectors of particle emission in the near-field surrounding spacecraft, detecting small particles at substantial distances and even providing limited ranging information.

The radiometer traces of Figure 1 permit some this particle's characteristics to be determined. Each of the radiometer detectors has a 3 mr field of view along its long axis. Because all the detectors observe similar particle intensity levels, the particle's blur circle is greater than 18 mr. This implies that the particle is closer than 7.5m distance from the radiometer array collection mirror (and greater than 50 cm distance for it to be outside of the telescope). The blur circle of the particle remains in the 18 mr field of view for about 8s. This corresponds to transverse velocity at least 2.2 mr/s. If the particle were at 7.5m distance, this would correspond to a 2 cm/s transverse velocity. Because the particle blur circle overfills the array, no information about the velocity along the optical axis can be extracted.

The spectral distribution of this particle was shown in Figure 3 and is reproduced in Figure 6. The broad spectral distribution has an average value of 9×10^{-5} W/cm^2-sr-μm that compares favorably with the $\approx 6 \times 10^{-5}$ W/cm^2-sr-μm value observed by the radiometers in their 8.4 to 17.6 μm bandpass.

Modeling of particle equilibrium temperatures[10,11] determined that particles will leave surfaces with the Shuttle surface temperature (~300 K) and in a characteristic time reach a new equilibrium determined by its optical

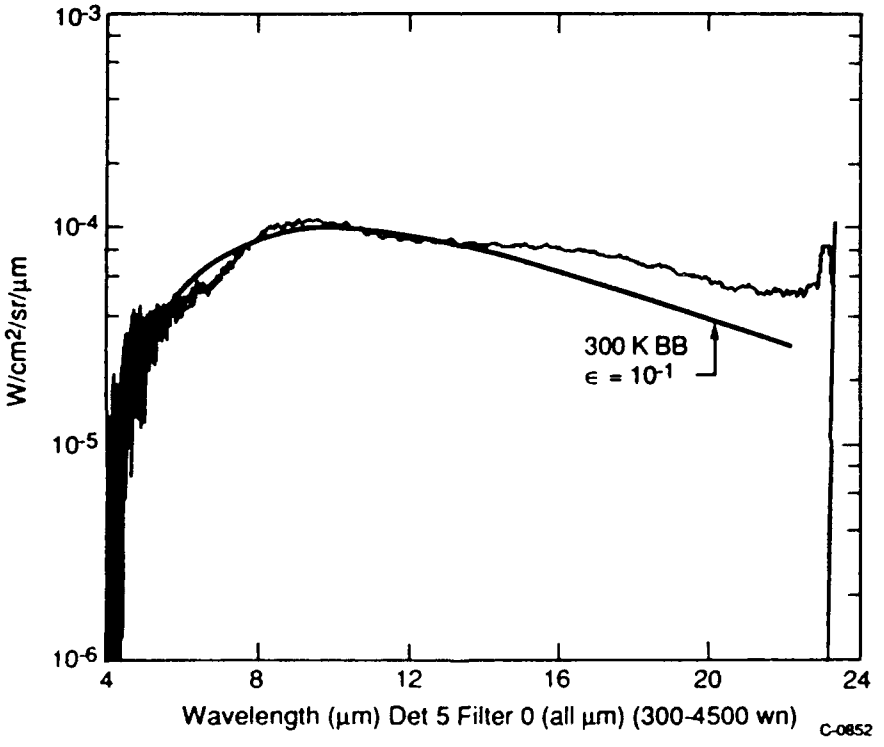

Fig. 6. Comparison of data in Fig. 3 with 300 K blackbody distribution having an emissivity of 0.1.

constants and the radiative environment. Typical equilibrium values are in the 200 K range. Shown in Figure 6 for comparison is the spectral distribution of a 300 K blackbody with an emissivity of 0.1. Thus the particle is as bright as a blackbody effectively filling 10% of the CIRRIS aperture. The particle's radiance is non-Planckian, having enhanced LWIR emission. All three spectra of this particle exhibit similar shapes. Because the particles radiance will be determined by reflected earthshine as well as self-emission, Figure 7 compares the particle's spectrum to a spectrum of the hard earth obtained at similar latitudes later in the mission. The hard earth spectrum is plotted in absolute units. Although this spectrum was not taken at the same time as the particle was observed, and thus may not completely represent the upwelling earthshine component, it is clear that the particle radiance is only about a factor 5 weaker than the brightness of the solid earth across the entire 9 to 20 μm bandpass. The particle's radiance distribution is driven by its thermal emission as tempered by its structured optical constants and by reflected earthshine.

In order to permit a better interpretation of the observed radiances levels, we require predictions of the radiances expected from single particles as a function of size and composition. In the companion paper, we have presented the details of our Mie scattering/emission predictions used for our treatment of a wide variety of the particles likely to be encountered by orbital sensors: ices, oxides, metals, paints.[11] Earthshine will control the particulate radiation and IR scattering signatures with negligible diurnal effects, while the sun contributes to the UV and visible scattering and increased thermal self-emission on the dayside. The spectral radiant intensity in W/sr-μm is simply the sum of the solar, earthshine, and self emission terms.

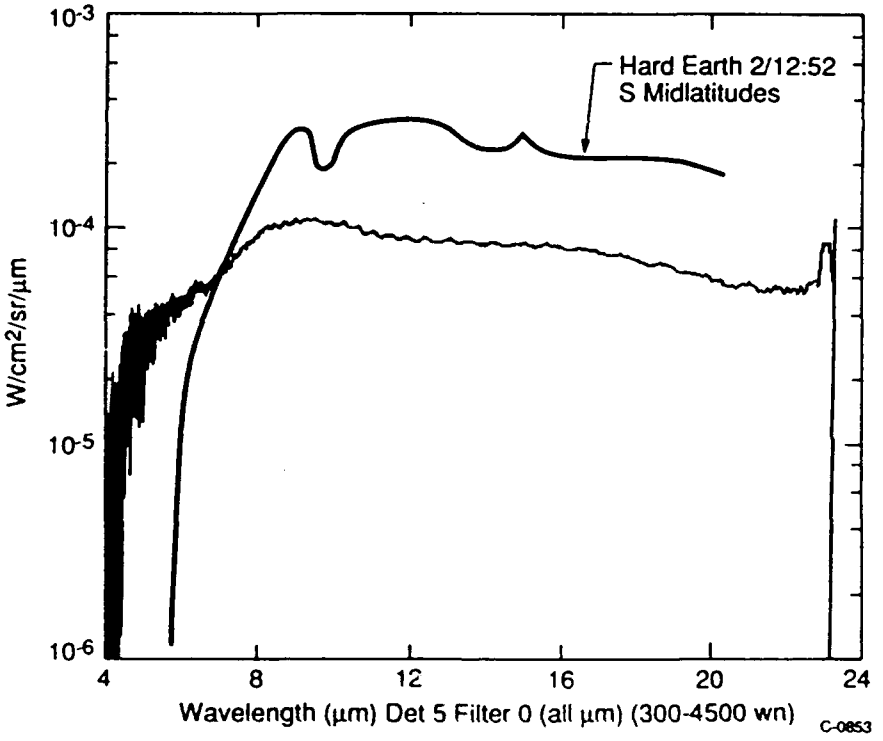

Fig. 7. CIRRIS-1A IF spectrum at 1/3:47:32 and hard earth spectrum.

The single particle brightness spectra were predicted from their self-emission and from the scattered solar and earthshine emission. The upwelling earthshine was treated as an extended source providing a realistic scattering signal estimate containing contributions of forward and backward scattered earth radiation from the horizons. The self-emission of each size particle was calculated from its equilibrium temperature in radiative steady state driven by the

radiative environment and its wavelength dependent scattering/extinction coefficients. Particles are expected to leave the spacecraft surface at the surface temperature. The smallest particles will come to the new radiative equilibrium temperature rapidly (in seconds), while particles above 100 μm require equilibration times approaching 30 min (and depend on the thermal conductivity within the particle). In general, equilibrium values around 200 K are calculated but the actual value will depend on solar illumination conditions, latitude, and the particle size.

Among the eight compositions modeled, the scattered intensity predictions for carbon were chosen to compare to the smaller particle radiance (Figure 8). The prediction for the radiance of a 30 μm carbon sphere exhibits the same broad shape and enhanced LWIR signature as the data, but does not match it perfectly. Moreover, the data is an order of magnitude brighter. Radiance scaling suggests that the particle observed at 1/3:47:54 was 120 ± 35 μm in size. For this type of particle the CIRRIS-1A unaveraged detection threshold would be 50 μm. It is dangerous to extrapolate our predictions for small particles to much larger sizes. As the particle size increases, the scattering efficiency extends well into the infrared, and the IR absorption substantially increases and loses spectral structure. Thus, composition determination of the larger particle will require further calculations.

Nevertheless, the current predictions were extrapolated to larger sizes assuming that the particle becomes a surface scatterer. Both the radiometers and the interferometer intensities suggest that the particle of Figures 1 and 3 is 5 ± 1.4 cm in size. The observed distribution is neither entirely Planckian nor reflected earthshine. Moreover, the spectrum changes with time indicating that the particle rotates, exposing different materials toward the sensor as it moves across the field of view. Based on the demonstrated CIRRIS-1A noise levels, this particle would have been detectable above the background level out to a range of 50 km.

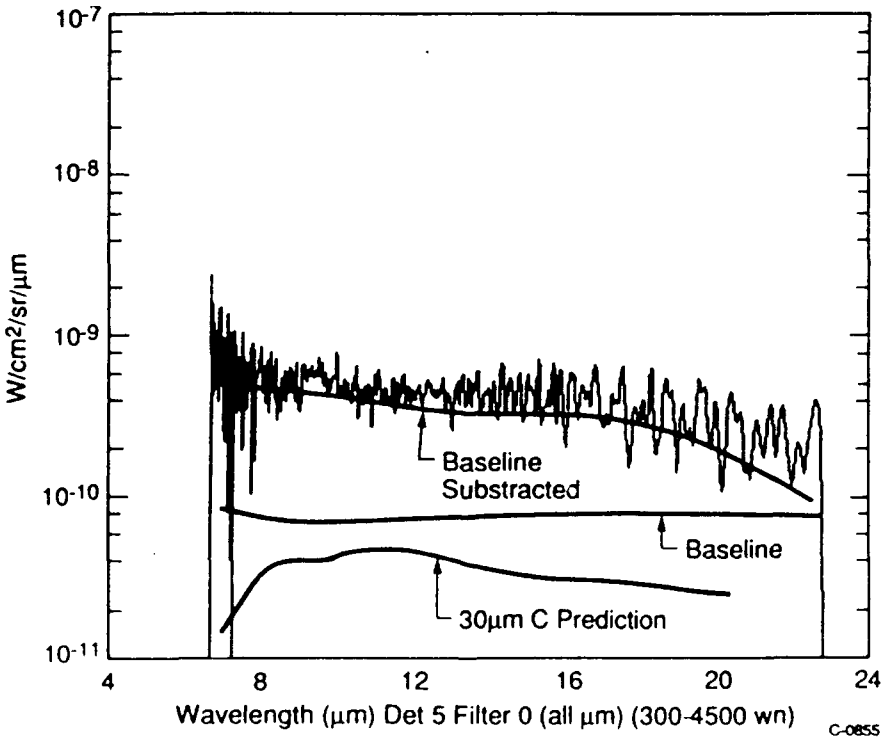

Fig. 8. CIRRIS-1A IF spectrum at 1/3:47:54 as compared to modeled carbon particle emission.

4. CONCLUSIONS

The optical environment during the CIRRIS-1A mission on STS 39 was generally quite benign. The careful ground handling and processing procedures appear to have successfully reduced contamination to an acceptable level. Orbital operations (such as the early time bakeouts and data acquisition during thruster disabled times viewing in the wake) were performed to minimize contamination effects. Nevertheless several discrete particle events were observed. We have reported here the analysis of particles observed after 27 hours on-orbit, after about 2 hours, 20 min of CIRRIS-1A data acquisition. Particle distance and transverse velocity were bounded based on the blur circle and the residence time in the field of view. Particle size and composition were estimated based on modeled signatures. The observed particles were in the cm and hundred μm range. The particle size threshold for CIRRIS-1A is estimated to be about 50 μm (without averaging).

The spectral resolution afforded by the interferometer will permit a better determination of the particle composition. The spectral resolution permits a more careful assessment of contamination levels and sources and thus can guide appropriate remedial actions.

The large particle observed here would be out of focus at all distances less than ~ 50m. However, if it had remained in the sensor field of view, it would have been detectable out to ranges of 50 km as a structured background in the interferometer scans and as an excess radiance in the radiometer signals.

Thus, optical instrumentation will permit assessment of the success of contamination prevention through careful ground handling procedures. These sensors will also permit the continuous measurement of the orbital production mechanisms (such as impacts, abrasion, and erosion) during long term spacecraft missions. Identification of the generation rates and sources will guide future space systems designers.

5. ACKNOWLEDGEMENTS

This effort was supported by the Strategic Defense Organization through a contract with the Applied Physics Laboratory of the Johns Hopkins University.

6. REFERENCES

1. B.D. Green et.al., "The Determination of the Spacecraft Contamination Environment," AFGL-TR-87-0303, 1987.

2. K.S. Clifton and J.K. Owens, "Optical Contamination Measurements on Early Shuttle Missions," Applied Optics 27, 603, 1988.

3. E.R. Miller, ed, "STS-2,-3,-4 Induced Environmental Contamination Monitor (IECM) Summary Report," NASA Tech. Memo 82524, 1983.

4. B.D. Green, G.K. Yates, M.A. Ahmadjian, and H. Miranda, "The Particle Environment Surrounding the Shuttle as Determined by the PACS Experiment," Proc. SPIE 777, 2, 1987.

5. D.W. Schuerman, D.E. Beeson, and F. Giovane, "Coronagraphic Technique to Infer the Nature of the Skylab Particulate Environment," Appl. Opt. 16, 1591, 1977.

6. J.J. Scialdone, "Particle Contaminant Relocation During Shuttle Ascent," NASA/GSFC Tech. Memo 87794, 1986.

7. D. McKeown, J.A. Fountain, V.H. Cox, and R.H. Peterson, "Analysis of TQCM Surface Contamination Adsorbed During the Spacelab 1 Mission," AIAA Paper 85-7008 in Shuttle Environment and Operations II Meeting, 1985.

8. M. Ahmadjian, R.M. Nadile, J.O. Wise, and B. Bartschi, "CIRRIS-1A Space Shuttle Experiment," J. Spacecraft 27(6), 669, 1990.

9. R. Narcisi, E. Trzcinski, G. Federico, L. Wlodyka, and D. Delorey, "The Gaseous and Plasma Environment Around the Space Shuttle, Proc. of the AIAA Shuttle Environment and Operations Meeting, 183, 1983.

10. W.T. Rawlins and B.D. Green, "Spectral Signatures of Micron-Sized Particles in the Shuttle Optical Environment, Applied Optics 26, 3052, 1987.

11. B.D. Green, "Optical Signatures of Particles in Space," SPIE Optical System Contamination III 1754, 1992.